Engineered Chemical Nanotopographies: RAFT Mediated Grafting of Anisotropic Poly(acrylamide) Patterns on Poly(dimethylsiloxane) to Modulate Marine Biofouling

Cary A. Kuliasha,†, Rebecca L. Fedderwitz†, John A. Finlay§, Sofia C. Franco§, Anthony S. Clare§, and Anthony B. Brennan†*

Department of Materials Science and Engineering, University of Florida, Gainesville, FL, USA.†

School of Natural and Environmental Sciences, Newcastle University, Newcastle-upon-Tyne, NE1 7RU, UK. §

ABSTRACT

Effectively negating the deleterious impact of marine biofouling on the world's maritime fleet in an environmentally conscientious manner presents a difficult challenge due to a variety of factors including the complexity and diversity of fouling species and the differing surface adhesion strategies. Understanding how surface properties relate to biofouling can inform and guide the development of new anti-biofouling coatings to address this challenge. Herein, we report on the development of a living photopolymerization strategy used to tailor the surface properties of silicone rubber using controlled anisotropic poly(acrylamide) patterns and the resulting anti-biofouling efficacy of these surfaces against zoospores of the model marine fouling organism, *Ulva linza*. Chemical patterns were fabricated using reversible addition-fragmentation chain-transfer

(RAFT) polymerization in conjunction with photolithography with pattern geometries inspired by the physical (i.e., non-chemical) Sharklet™ engineered microtopography system that has been shown effective against the same model organism. Sharklet chemical patterns and analogous parallel channels were fabricated with sizes ranging from 2-10 μm in the lateral dimension and tailorable feature heights ranging from 10's to 100's of nm. Non-patterned, chemically grafted poly(acrylamide) silicone surfaces inhibited algal spore attachment density by 59% compared to the silicone control; however, the chemical nanotopographies were not statistically different from the control. While these results indicate that the chemical nanotopographies chosen do not represent an effective anti-biofouling coating, it was found that the Sharklet pattern geometry, when sized below the 5 μm critical attachment size of the spores, significantly reduced the algal spore density compared to the equally sized channel geometry. These results indicate that specific chemical geometry of the proper sizing can impact the behavior of the algal spores and could be used to further study the mechanistic behavior of biofouling organisms.

INTRODUCTION

Marine biofouling is the undesirable attachment and growth of organisms such as bacteria, algae, and invertebrates on surfaces, and it is a leading and continuing problem for various maritime industries. It has a number of undesirable effects including increased maritime shipping costs,[1,2] introduction of invasive species into local ecosystems,[3] and reduced efficiency for power generation and water filtration facilities.[4] The properties of the fouling surface and characteristics of the fouling vector are the primary factors that govern fouling severity and strength of the biofouling interface, and better understanding the most effective and environmentally friendly strategies to combat biofouling holds the potential to drastically reduce both the human and material costs of this pernicious global problem. To this end, researchers are studying the impact

of various surface properties including surface free energy (SFE) and wettability,[5–7] chemistry,[8] micro/nano roughness,[9] and charged chemical groups[10,11] on the antifouling (AF) and fouling-release (FR) efficacy of surfaces; however, the exact impact of specific surface properties on the macroscale biofouling response is typically complicated by competing and difficult to control properties that make it challenging to determine the most effective anti-biofouling strategy to employ.[12,13]

Engineering surfaces with either physical or chemical patterns with controlled geometries, dimensions, roughness, etc. offers an excellent platform to study biofouling because patterns allow for the precise tuning of relevant surface properties that can limit conflicting variables.[9,14–16] Our research group has shown that physically textured surfaces modified with the Sharklet™ engineered microtopography, which was inspired by the placoid scales of sharks,[17] can inhibit surface fouling by marine algae by 86%[17] and marine bacteria by >99%[18] (compared to non-textured controls), inhibit *Staphylococcus aureus* biofilm formation,[19] and even promote wound healing[20] by controlling the thermodynamics of the organism-surface interaction.[16] The Sharklet™ geometry has been found to be unique in its effectiveness compared to equivalently sized patterns of parallel channels or pillars,[9] and modification of the standard Sharklet™ pattern geometry and dimensions can be used to modulate the attachment density of various fouling species informed by the surface energetics attachment (SEA) model.[16] The SEA model utilizes surface thermodynamics and attachment point theory to accurately predict fouling attachment density (promotion or inhibition) between different patterns and a variety of organisms. However, physically textured substrates, such as Sharklet™, are limited in their antifouling efficacy when the relative size difference between the fouling organism and pattern is large,[21] and as such they do not currently

represent a broad-spectrum antifouling strategy when multiple different fouling vectors are present.

Modifying surfaces with polymeric chains of varying chemistries has been shown to be another effective anti-biofouling strategy,[22] and chemical patterns that use AF chemical moieties[23–26] can be used to modulate and guide fouling responses. For example, patterning substrates with non-fouling materials like poly(ethylene glycol) (PEG) derivatives[23,26] and then growing cells on the fouling substrate has been used to isolate cells into contained "islands" or channels in order to study cellular microenvironments and processes. The macroscale antifouling performance of chemically patterned substrates is typically based on surface area arguments where fouling vectors avoid the AF chemistry and instead attach to the surrounding non-modified fouling background.[23,24] Many studies have used chemical patterns to isolate the behavior of fouling vectors to better understand attachment strategies, relationship with SFE, and impact of other surface properties. However, there has been limited information on the specific effects of pattern geometry on the macroscale fouling of organisms that cannot be accounted for by simple surface area arguments, and we believe that the unique Sharklet™ geometry is an excellent candidate for this type of study.

The objective of this study was to investigate the efficacy of anisotropic poly(acrylamide) (P(AAm)) chemical nanotopographies that utilize lateral geometries inspired by the Sharklet™ AF physical microtopography, in addition to analogous parallel channels, to inhibit surface fouling by zoospores of the common marine fouling algae *Ulva linza*.[27] We have long known that the specific geometry of the physical Sharklet™ microtopography effectively controls the local environment that prevents biofouling in ways not obtained with analogous channels or pillars commonly used

by other research groups,[9] and we hypothesize that similar chemical topographies may have similar unique effects that have not been realized before.

The substrate of choice for this study was a poly(dimethylsiloxane) elastomer (PDMSe) that has been widely used by research groups studying physical microtopographies due to its compatibility with an array of molding/patterning techniques.[9,17,28] PDMSe is also biocompatible[29] and has been extensively employed by the anti-biofouling research community due to its low SFE and low modulus that makes it an excellent standard control for both AF and FR studies against common marine algae, diatoms, tubeworms, hydrozoans, barnacles, and mussels.[22] P(AAm) was chosen because of its AF efficacy against the chosen fouling organism (unpublished author work) resulting from its strong binding affinity to water in a fashion similar to PEG. The grafting strategy chosen to form the P(AAm) patterns on PDMSe utilizes an established UV-photolithography protocol catalyzed by a benzophenone (BP) surface initiator coupled with a reversible addition-fragmentation chain transfer (RAFT) living-polymerization technique recently developed and discussed in detail.[30] The RAFT strategy polymerizes P(AAm) to high conversions (>98%) with tailorable molecular weight and low dispersity ($Đ<1.1$) making it an excellent grafting strategy that allows for the surface characteristics of the patterns to be easily controlled.[30]

Zoospores of the green algae *U. linza* were chosen to test the anti-biofouling properties of the fabricated anisotropic chemical nanotopographies because they are motile in the water column and actively probe surfaces in search of the most suitable attachment sites making them ideal candidates to reveal potential differences between chemical nanotopography geometries.[27] *U. linza* and smooth PDMSe coatings have also been used in many previous studies by the marine fouling community to assess AF performance of new coatings,[22,31] and it was chosen to maintain these standards to allow for comparisons between the current study and fouling research performed over

the past ~20 years. The lateral dimensions of the chemical patterns were chosen to range from 2–10 μm because 5 μm[9,24] is the approximate critical size dimension of the zoospores and this range encompasses the same size scale used for engineered microtopographies both above and below.

MATERIALS AND METHODS.

Materials

Borosilicate glass slides (76 mm x 25 mm x 1 mm) were purchased from Fisher Scientific (Hampton, NH, USA). Platinum-catalyzed Xiameter™ RTV-4232-T2 two-part PDMS resin was purchased from Dow Corning (Midland, MI, USA). Allyltrimethoxysilane (ATS, >98%), benzophenone (BP, >99%), acrylamide (AAm, >99%), and 2-hydroxy-4′-(2-hydroxyethoxy)-2-methylpropiophenone (Irgacure 2959, 98%) were purchased from Millipore-Sigma (Burlington, MA, USA). 2-(1-carboxy-1-methyl-ethylsulfanylthiocarbonylsulfanyl)-2-methyl-propionic acid (CMP) was used as the RAFT chain transfer agent (CTA) and synthesized according to Lai et al.[32] AAm was recrystallized 3x from chloroform to remove impurities and vacuum-dried, BP was recrystallized 3x from acetone and vacuum-dried, and deionized water (DIW, 18.2 MΩ-cm) was produced in house using a Milli-Q system (Millipore-Sigma, Burlington, MA, USA). All other materials were used as received.

PDMSe Substrate Preparation

Glass slides were cleaned by a propane torch, reacted with a solution of 5% ATS (vol.%) in 95% ethanol acidified with glacial acetic acid to pH=4.5, washed with ethanol, and dehydrated at 120 °C. PDMS was prepared by mixing 10:1 (wt.%) resin to curing agent and degassed under vacuum. The mixture was poured over ATS-glass slides and cured for 24 h at room temperature between two poly(ethylene terephthalate) coated plates with 1.6 mm spacers resulting in 600 μm thick

PDMSe-coated glass slides. A razor blade was used to liberate PDMSe glass slides from the PDMSe sheet.

Photomask Fabrication

Pattern photomasks were designed using Layout Editor software (Juspertor GmbH, Unterhaching, GER) and exposed onto chrome-quartz photomasks (Nano-Film Microcircuit Technology, Westlake Village, CA, USA) using a DWL 66FS laser writer (Heidelberg Instruments GmbH, Heidelberg, GER). Exposed masks were developed in AZ400K (MicroChemicals GmbH, Ulm, GER) and etched in chrome etchant 1020 (Transene Company, Inc., Danvers, MA, USA). Three photomasks were made with each containing three different 225 mm^2 patterned regions spaced 10 mm apart. The three patterned regions consisted of parallel channels, Sharklet_n4, and Sharklet_n10 geometry with features and spacings of 2, 5, or 10 μm (see *Photopatterned Nomenclature* below).

PDMSe RAFT Photopatterning

The RAFT PDMSe grafting protocol from Kuliasha et al.[30] was adopted for photopatterning (Sch. 1). Briefly, a RAFT monomer solution was prepared in DIW with 3 M AAm ($[M_0]$), 3.75 mM Irgacure 2959 ($[I_0]$), and 3.75 mM CMP ($[CTA_0]$) and degassed by bubbling N_2. Glass slide PDMSe substrates were immersed in a 10 wt % BP solution in methanol to impregnate the substrate with a BP surface photoinitiator. The degassed pre-polymer solution was pipetted onto the dried BP-PDMSe substrate, evenly distributed by a patterned photomask, and UV polymerized using a 10 mW/cm^2 Lesco CureMax FEM1011 UV curing system (JH Technologies, Bradenton, FL, USA) resulting in P(AAm) photografted PDMSe (P(AAm)-g-PDMSe). RAFT polymerization allowed for the molecular weight and resultant height of patterned grafts to be modified by varying UV treatment time from 2-8 min. Grafted substrates were cleaned of residual AAm monomer, non-

grafted P(AAm), and CMP/ BP initiators by successive washes/ soaks in DIW and methanol for 48 h. Cleaned P(AAm)-g-PDMSe samples were stored in DIW at 4 ˚C until required for analysis. Grafting was restricted to three 225 mm^2 patterned areas on the PDMSe surface as governed by the photomasks. Non-patterned P(AAm)-g-PDMSe samples were fabricated according to the same procedure using quartz plates in place of the photomask (ground and polished, 3.5 in x 3.5 in x 0.062 in, Technical Glass Products, Painesville, OH, USA).

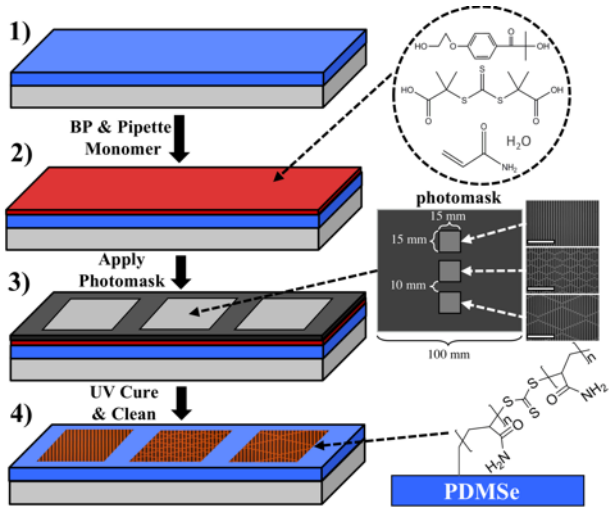

Scheme 1. RAFT photopatterning schematic used to fabricate P(AAm)-g-PDMSe surfaces attached to glass microscope slides. (1) As-cured PDMSe (blue) attached to glass slide substrate (grey) is (2) impregnated with BP and coated in a RAFT pre-polymer solution (red and inset) that is subsequently (3) UV cured using a photomask (grey and inset) resulting in a (4) PDMSe sample that after cleaning contains three regions of surface grafted, anisotropic P(AAm) chemical nanotopographies (red) surrounded by non-patterned PDMSe regions (blue).

Photopatterned Nomenclature

Grafted PDMSe samples are labeled in this work as P(AAm)-g-PDMSe, with included pattern designation using the following format: 'SK' indicates the same geometric footprint as the Sharklet™ engineered microtopography, and 'CH' refers to parallel channels. Patterned feature

width and spacing dimensions are reported in microns while feature height is reported in nanometers. Finally, '_n#' refers to the number of unique repeating features within the Sharklet pattern's unit cell. For example, 150SK2x2_n4 indicates a 150 nm tall chemical nanotopography with 2 μm lateral features spaced 2 μm apart resembling Sharklet™ topographies with 4 unique repeated features:

(Height) (Geometry) (Feature Width)x(Feature Spacing)_(# Unique Features)

Surface Analysis

ATR-FTIR Spectroscopy was performed on vacuum dehydrated PDMSe samples using a Nicolet 6700 FT-IR spectrometer (Thermo Scientific, Waltham, MA, USA) equipped with a germanium crystal. A total of 128 scans per spectrum were acquired with a resolution of 4 cm^{-1}. A background spectrum in air was collected and subtracted from the sample spectrum. A Dimension Icon AFM (Bruker, Billerica, MA, USA) was used to analyze the surface morphology of samples fully immersed in DIW using ScanAsyst® fluid+ tips (Bruker) in ScanAsyst® mode. NanoScope Analysis software (Bruker) was used to calculate pattern dimensions and surface nanoroughness. Pattern heights were determined by measuring the height sensor's peak-to-valley difference on 12 spots per scan between three 93 x 93 μm AFM scans on 3 sample replicates per pattern type and UV polymerization time. A model A100 goniometer (Ramé-Hart Instrument Co., Succasunna, NJ, USA) was used to measure the static water contact angle (CA) of 5 μL DIW droplets applied to sample surfaces via a glass micropipette. Samples were dried of residual DIW with N_2 gas prior to CA measurements, and 5 individual droplets were measured on each sample surface.

U. linza Bioassay

Patterned P(AAm)-g-PDMSe samples were fabricated according to Sch. 1 consisting of three 225 mm_2 patterned regions containing nanotopographies with lateral dimensions of 2x2, 5x5, or 10x10 (μm x μm). Each lateral dimension sample group was replicated (n=4) resulting in a total of 9 different patterns. Non-patterned P(AAm)-g-PDMSe and non-grafted PDMSe coatings were fabricated as controls (n=4). Test coatings were sterilized by three successive washes in 70% isopropanol and shipped to Newcastle University, UK in sterile centrifuge tubes filled with 0.2 μm filtered DIW.

The sample cohort was tested for AF efficacy with a *U. linza* algal zoospore attachment bioassay. Coatings were equilibrated in 0.22 μm filtered artificial seawater (ASW) for 24 h prior to testing. Algal zoospores of *U. linza* were obtained from mature plants using a standard method.[21] A suspension of zoospores (10 ml; $1x10^6$ spores/ml) was added to individual compartments of quadriPERM dishes containing the samples. After 45 min in darkness at 20 °C, the slides were washed by passing 10 times through a beaker of ASW to remove unsettled (i.e., swimming) spores. Slides were fixed using 2.5% glutaraldehyde in ASW. The density of zoospores attached to the surface was counted using Axiovision 4 software attached to a Zeiss Axioskop fluorescence microscope. Spores were visualized by autofluorescence of chlorophyll. Counts were made for 30 fields of view (each 0.15 mm^2) on each patterned region. The entire bioassay procedure was performed twice on separate sample cohorts fabricated two months apart in order to determine batch-to-batch and bioassay variability.

RESULTS AND DISCUSSION

Chemical Nanotopography Analysis

Successful UV-initiated grafting of P(AAm) onto PDMSe was verified with ATR-FTIR analysis as evidenced by the appearance of primary amine (3379 and 3202 cm^{-1}) and amide I and II (1664

and 1614 cm-1) peaks (Fig. 1 and SI). IR peaks corresponding to P(AAm) became more prevalent at increasing UV times due to the increased molecular weight and feature height of the P(AAm) patterns (discussed below). Impregnating PDMSe with BP using methanol as the carrier solvent results in a % mass change < 0.2%,[30] and PDMSe is highly immiscible to water used as the monomer carrier solvent. Therefore, it can be safely assumed that P(AAm) grafting was relegated to the top surface of the PDMSe with minimal penetration of P(AAm) within the bulk PDMSe. Optical and AFM inspection confirmed that the photolithographic technique was successful at creating the full range of targeted chemical nanotopographies with lateral features governed by the photomask design (Fig. 2 and SI). AFM was the primary method used to analyze the pattern morphology because of the high spatial resolution and ability to measure nanometer scale feature heights of substrates fully submerged in DIW thus ensuring complete P(AAm) graft layer hydration.

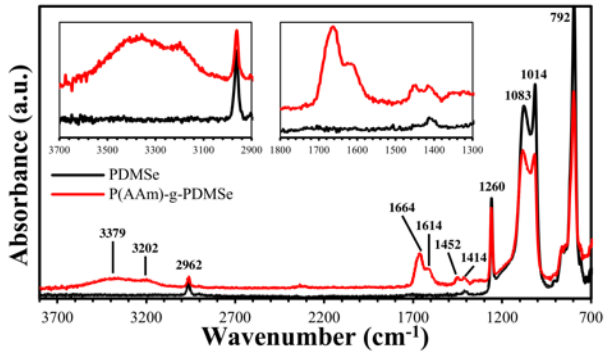

Figure 1. ATR-FTIR spectra of as-cured PDMSe (black) and P(AAm)-g-PDMSe (red). P(AAm) grafting is evidenced by new peaks corresponding to the amide I and II and primary amine absorption bands (insets) of P(AAm) that are not present in as-cured PDMSe.

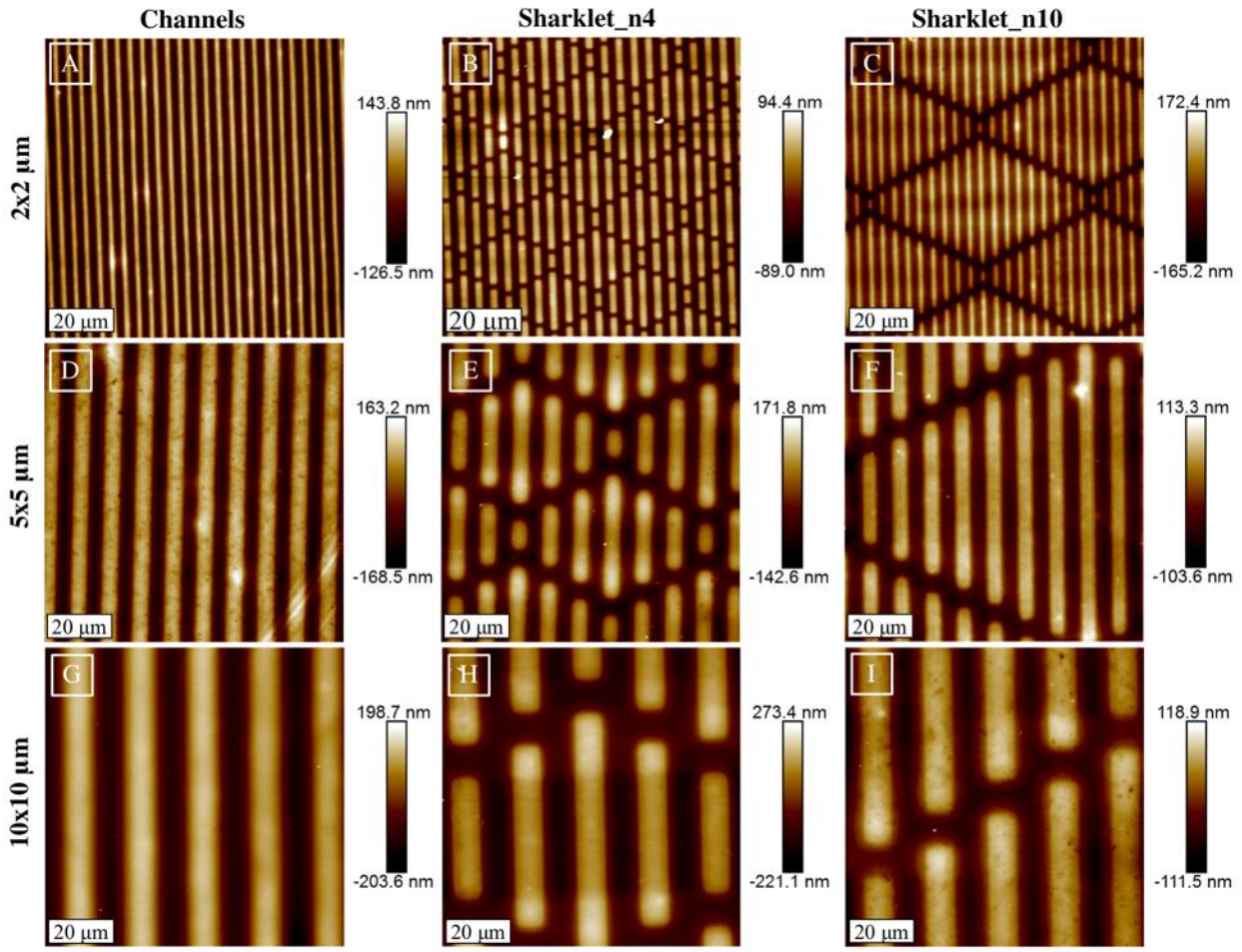

Figure 2. Representative 2D AFM height sensor scans of P(AAm)-g-PDMSe surfaces immersed in DIW. (A) CH2x2, (B) SK2x2_n4, (C) SK2x2_n10, (D) CH5x5, (E) SK5x5_n4, (F) SK5x5_n10, (G) CH10x10, (H) SK10x10_n4, and (I) SK10x10_n10. Each row represents a different lateral spacing group (2x2, 5x5, or 10x10 µm) and each column represents different pattern geometries (Channels, Sharklet_n4, or Sharklet_n10). All scans are approximately 93x93 μm^2.

An initial ~2-3 min UV inhibition period, during which minimal photografting occurred, generated patterns that were less than 10 nm tall. During the inhibition period, no significant polymerization occurred because the majority of UV-initiated radicals in solution and on the PDMSe surface fragment the RAFT CTA forming macroCTA radicals[33] instead of polymerizing available monomer as expected for typical chain-growth reactions. Appreciable living

polymerization of monomers only occurs after available CTA has been converted to macroCTAs and RAFT equilibrium has been reached.[33]

Reaction kinetics of BP-modulated RAFT photografting is complicated by the ability of BP to abstract tertiary α-C from the backbone of AAm to produce a branched polymer graft as opposed to a strictly linear chain causing deviations from traditional RAFT living chain-growth polymerization.[30] Due to this branching effect of the grafted polymer, the precise evolution of surface graft molecular weight is not readily analyzable. Therefore, grafted pattern feature height was studied instead and used as an analog to graft molecular weight. However, non-grafted P(AAm) collected from solution (i.e., primarily linear, non-branched polymers) exhibits a linear evolution of molecular weight of ~5.7 kDa/min after a 3 min inhibition period resulting in 99% conversion after 20 min.[30] This reaction rate can be considered as the upper limit for the photopatterning reaction.

AFM analysis of surfaces submerged in DIW was used to determine grafted feature height and surface nanoroughness in their fully swollen/hydrated state as a function of UV polymerization time for all fabricated pattern geometries (Fig. 3 and SI). Surfaces were not characterized in their dry state because the *U. linza* AF tests were performed in aqueous/marine environments, and testing was chosen to replicate the application environment. The average feature height as a function of increasing UV time for features with lateral dimensions of 2x2, 5x5, and 10x10 (μm x μm) fit a linear regression (R^2 values of 0.999, 0.995, and 0.951, respectively). This analysis combined pattern geometries of CH, SK_n4, and SK_n10 within the same lateral dimension group because there was determined to be no effect of pattern geometry on polymerization rate or feature height. Living polymerization reactions exhibit pseudo first-order kinetics of molecular weight versus conversion and polymerization time,[33] and the linear relationship of grafted feature height

as an analog to molecular weight versus UV time indicates that the living chain-growth RAFT moderated photografting was successful.[30] However, narrower features polymerized at slower rates due to the difference in the area exposed to UV irradiation during grafting. Increasing the lateral pattern dimensions from 2x2 to 5x5 to 10x10 caused the pattern height to increase from 49, 67, and 129 nm/min, respectively. The R_{RMS} nanoroughness for these patterns also showed a linear relationship (R_2=0.991) with increasing feature height irrespective of pattern geometry or lateral dimension (Fig. 3).

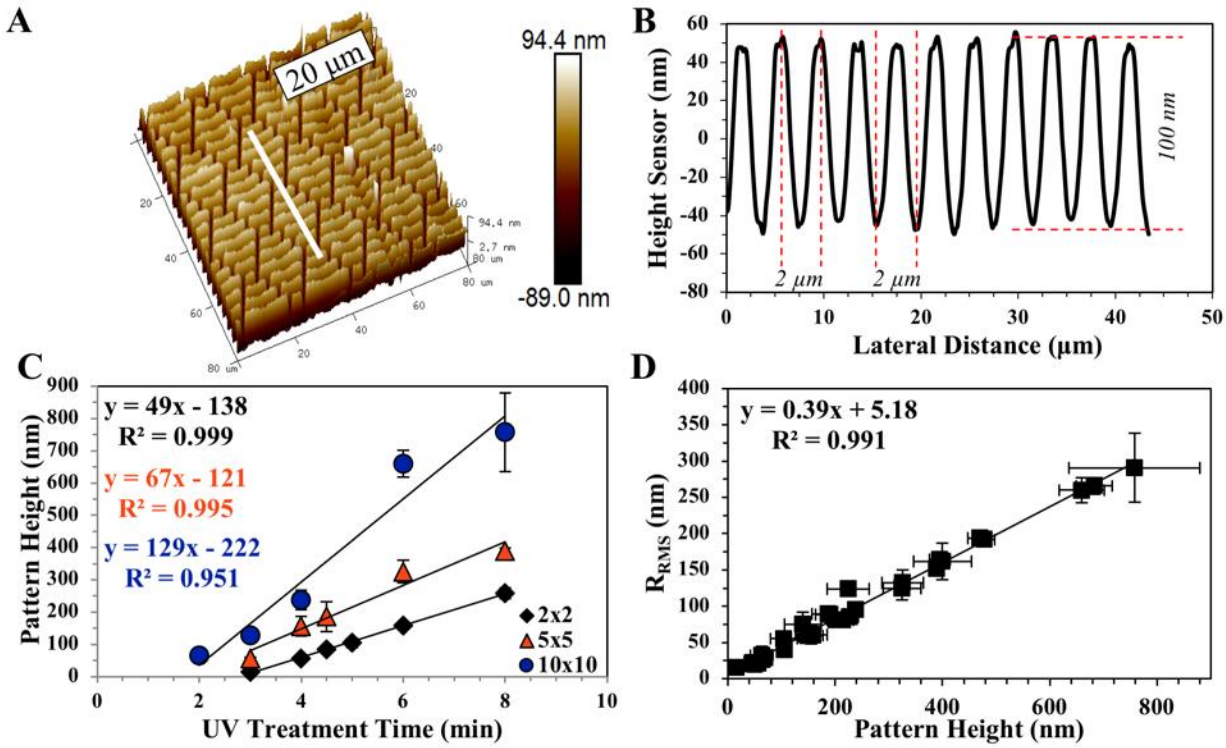

Figure 3. Summary of AFM data collected from chemical nanotopographies with lateral size ranging from 2 to 10 µm. (A) Representative 3D AFM scan of a 100SK2x2_n4 surface with an overlaid line scan (white). (B) AFM height sensor vs. lateral distance of a line scan taken from (A) showing both the height and feature spacing (dashed lines). (C) Compilation of the feature height vs. UV treatment time for all patterns. Feature heights were consistent across the three different geometries within the same lateral space group for a given exposure time. Linear regression

analysis was performed on each lateral dimension group and the results are shown in the inset. (D) R_{RMS} nanoroughness vs. measured feature height calculated from 93x93 μm^2 AFM scans. Data points represent the arithmetic mean (± standard deviation) of 12 line scans on 3 replicate samples (n=12, N=3).

The non-patterned P(AAm)-g-PDMSe surface exhibited a controllable decrease in static water CA with increasing UV time to a minimum of 55˚ ± 6˚ after 8 min UV due to increasing P(AAm) molecular weight.[30] Conversely, water CA analysis of all surfaces patterned with hydrophilic P(AAm) nanotopographies showed only a modest decrease of ~ 4 to 11° compared to native PDMSe (110°) irrespective of variations in pattern geometry (CH or SK), feature height (15–760 nm), or lateral dimension size (2–10 μm) (Tab. 1). This indicates that the hydrophobic PDMSe regions dominate the pattern's macroscopic surface wettability while the P(AAm) regions have only a minimal impact. It has been experimentally[34] and theoretically[35] shown that anisotropic chemical patterns with alternating hydrophilic/hydrophobic domains cause water droplets to elongate due to preferential wetting down the long axis of hydrophilic regions. This phenomenon is also prevalent with physical patterns[36] and has been attributed to differences in the energy barrier of wetting between the parallel or perpendicular pattern directions. It was expected that P(AAm) anisotropic nanotopographies would display differences in CA caused by such preferential wetting along the relatively hydrophilic P(AAm), but measuring patterns along the feature's long axis (parallel) or short axis (perpendicular) did not reveal any differences (Tab. 1).

Table 1. Static water CA of chemical nanotopographies measured parallel or perpendicular to the long axis of the topography feature direction.

	Sessile Drop Water Contact Angle (˚)

	Lateral Dimension and Measurement Direction					
Geometry	2x2 $_{\parallel}$	2x2 $_{\perp}$	5x5 $_{\parallel}$	5x5 $_{\perp}$	10x10 $_{\parallel}$	10x10 $_{\perp}$
CH	101 (4)	103 (3)	106 (3)	105 (2)	103 (4)	103 (3)
SK_n4	100 (4)	102 (2)	104 (4)	104 (4)	101 (3)	99 (3)
SK_n10	100 (3)	106 (2)	102 (5)	106 (2)	102 (6)	104 (3)

Data points represent the arithmetic average (standard deviation) of samples at four UV treatment times, n=3. Each sample was measured with 5 static droplets with angle measurements taken on both the left and right side of the droplet.

The Cassie-Baxter wetting theory has been applied to surfaces that demonstrate both solid-liquid and liquid-air interfaces along the contact area of the liquid droplet (e.g., physical topographies) or with chemistry$_1$-liquid and chemistry$_2$-liquid (e.g., chemically heterogenous topographies) interfaces (Eq. 1).[37,38] For this case using Eq. 1, $\theta_{*theoretical}$ represents the composite theoretical CA, θ_1 and θ_2 the experimental CA of the homogenous surfaces (grafted or non-grafted, respectively), and f_1 and f_2 their respective surface area fractions. This theory was applied to CH2x2 P(AAm)-g-PDMSe surfaces where $f_1=f_2=0.5$, θ_1 is the experimental CA of PDMSe, and θ_2 is the experimental CA of the analogous non-patterned P(AAm)-g-PDMSe surface (Fig. 4). The Cassie-Baxter theory predicts that the chemically patterned substrates would exhibit a decrease in CA with increasing UV time and feature height due to the decrease in the CA of the analogous non-patterned P(AAm)-g-PDMSe surfaces;[30] however, these predications do not hold true at UV times >6 min as the non-patterned P(AAm)-g-PDMSe CA decreases with increasing graft molecular weight (Fig. 4). These same conclusions can be drawn for the other P(AAm) nanotopographies. It is likely that the hydrophobic PDMSe domains pin the water contact line thus preventing the droplet from wetting the surface in the manner predicted by Cassie-Baxter.[38] It is clear from this behavior that the PDMSe domains dominate the local surface wettability and effectively pin the motion of water droplets.

$$\cos(\theta^*_{theoretical}) = f_1 \cos(\theta_1) + f_2 \cos(\theta_2)$$

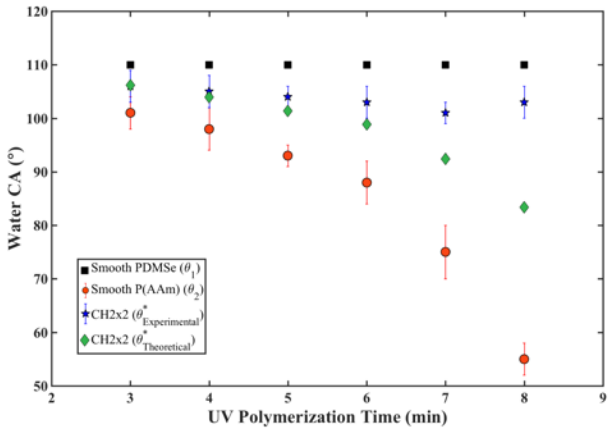

Figure 4. Water CA vs. UV polymerization time for experimentally measured surfaces including non-patterned P(AAm) (θ_2, red), CH2x2 ($\theta^*_{experimental}$, blue), and the theoretically predicated composite CA ($\theta^*_{theoretical}$, green) assuming a constant non-grafted PDMSe CA of 110 ˚ (θ_1, black) according to Eq. 1. Experimental data points represent the arithmetic average (± standard deviation), N=3, n=5

The RAFT photopatterning technique does have a maximum achievable pattern height of ~250 nm for the 2x2 patterns. UV polymerization time >8 min resulted in thickening of the 2 µm features as the grafts polymerized laterally across the surface (Fig. 5). Eventually a point was reached where the grafts bridged the 2 µm PDMSe region between adjacent P(AAm) features resulting in a surface that no longer resembled the proper pattern geometry with a corresponding decrease in the water CA <55˚, similar to non-patterned P(AAm)-g-PDMSe at equivalent UV treatment times. This limitation was not observed with the larger 5x5 or 10x10 patterns at >8 min UV; however, rigorous analysis of these patterns was not performed to pinpoint the onset of any pattern thickening.

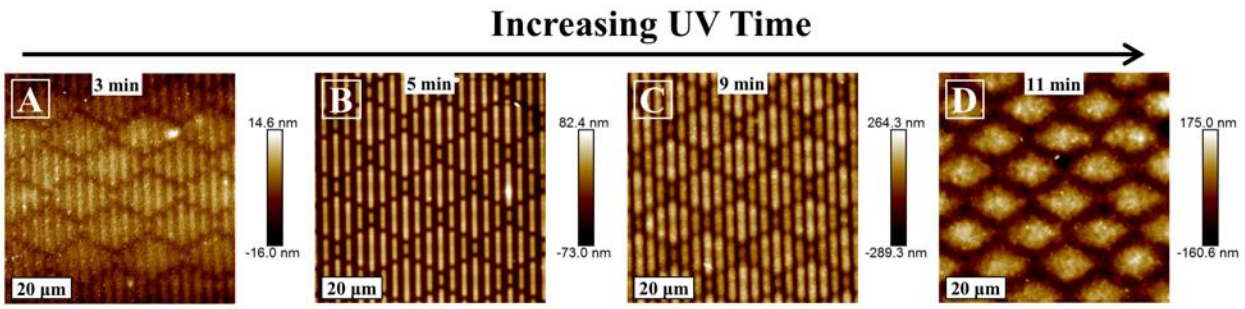

Figure 5. 2D AFM scans of SK2x2_n4 P(AAm)-g-PDMSe with increasing UV polymerization time showing the onset of pattern formation at 3 min after the RAFT inhibition period, followed by high-fidelity patterns from 3-8 min, and proceeding to gradual thickening of the patterns at 9 min with complete loss of independent features at 11 min.

AF Efficacy vs. Algal Zoospores of Ulva linza

P(AAm)-g-PDMSe with CH, SK_n4, and SK_n10 nanotopographies with feature dimensions of 2x2, 5x5, and 10x10 (µm x µm) were tested against zoospores of the common marine fouling green alga *U. linza* to determine the pattern's AF efficacy. In order to reduce variables, the 2x2, 5x5, and 10x10 patterned samples were UV treated for 6, 4, and 3 min respectively in order to produce patterns with equivalent feature heights of 132 nm ± 51 (arithmetic average ± standard deviation) resulting in chemical topographies with equivalent degrees of swelling and molecular weight. Non-patterned (i.e., smooth) P(AAm)-g-PDMSe coatings were also tested in order to determine the effect of a chemically homogenous surface, and these coatings were UV treated for 4 min to produce a water CA of 98° ± 3° equivalent to the chemically patterned substrates. Non-patterned (i.e., non-grafted, smooth) PDMSe samples with a water CA of 110° ± 2° were used as controls.

Non-patterned P(AAm)-g-PDMSe surfaces significantly inhibited the attachment density of algal zoospores by 59% compared to PDMSe controls during two separate bioassays ($F_{10,879}$ =

23.68, $p < 0.0001$) (Fig. 6). This reduction proves that P(AAm) is an effective AF chemistry against the zoospores; however, the overall % reduction was not as large as that achieved by a variety of other chemistries including hydrophilic PEG (88%)[39] and amphiphilic poly(co-acrylates) (85-92%),[40] compared to smooth PDMSe control. On the other hand, patterned P(AAm) nanotopographies, in the size range and geometries investigated, did not significantly change the attachment density of *U. linza* compared to the control (Fig. 6). As discussed previously, analysis of the water CA of the grafted nanotopographies revealed that the PDMSe regions dominate the macroscale wettability of the patterns, and it is likely that these same regions also control the macroscale fouling behavior. For the non-patterned surfaces, P(AAm) grafts conformally coat the entire sample surface, effectively blocking the influencing effect of the underlying PDMSe and resulting in significant inhibition of algal spores in a manner not evidenced by chemical nanotopographies with equivalent macroscopic static water CA.

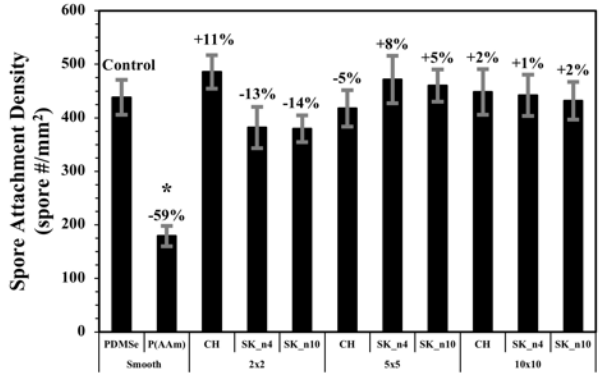

Figure 6. Attachment density of algal zoospores on different surfaces. Smooth P(AAm) showed a significant reduction in attachment density of 59% ($F_{10,879} = 23.68$, $p < 0.0001$) while the anisotropic nanotopographies were not statistical different from the control. Inset values indicate the % change in attachment density compared to the PDMSe controls. Data points represent the arithmetic average (± 95% confidence intervals) taken from 30 counts each on 8 replicates separated between two bioassays (4 replicates/bioassay).

Finlay et al. [24] reported for alternating PEG/fluorinated channels that *U. linza* attachment density was governed by competing factors including the hydrophilicity of the region surrounding the patterned area (i.e., background) and the individual pattern's size. Algal zoospore attachment density on patterned regions was similar to the fluorinated control irrespective of channel size/spacing, for dimensions ranging from 2 to 500 μm, when the background surrounding the patterned regions was fluorinated. However, when PEG backgrounds replaced the fluorinated background, the patterns dimensioned at 2 to 5 μm inhibited spore settlement in a fashion similar to homogenous PEG surfaces. Furthermore, it was shown that spores aggregated in higher densities on the hydrophobic fluorinated regions compared to hydrophilic PEG regions for channels 20 μm and larger, which is consistent with earlier assays on self-assembled monolayers.[41] It was concluded that the hydrophobic fluorinated regions attracted spores and dominated the global fouling effect, and only patterns sized at or below the spore's body size (i.e., 5 μm[9,24]) had a strong AF effect when the spores were not given attractive regions to settle (i.e., hydrophobic background) thus forcing them to search for alternative settlement areas. For the analysis presented here, the non-grafted PDMSe background surrounding the chemically patterned regions can be considered to be analogous to the fluorinated background. The P(AAm) nanotopographies were not sufficient to overcome the influencing effect of the hydrophobic PDMSe domains.

Despite this, nanotopography geometry and feature size/spacing did affect algal spore settlement to a limited degree. By comparing pattern geometry within the three different equally sized lateral groups, 2x2 patterned SK_n4 and SK_n10 statistically inhibited fouling to a greater degree than the CH2x2 geometry ($F_{2,239}$=11.14, $p<0.0001$) while all the 5x5 patterns ($F_{2,239}$=1.94, $p=0.146$) and 10x10 patterns ($F_{2,239}$=0.30, $p=0.741$) were statistically equivalent within their lateral size group irrespective of pattern geometry. These results indicate that the geometry of a chemical

pattern, when sized below the spore's critical attachment size of 5 μm,[9,24] can influence the attachment of algal zoospores, and this effect cannot be based on surface area coverage arguments alone. SK_n4 patterns have an AF grafted area of ~42% while the CH patterns have ~50% graft area coverage. Based on surface coverage arguments it would be expected that the SK patterns would have a higher attachment density if the relative surface area of fouling PDMSe to AF P(AAm) was the only important parameter; however, this is not the case. The specific Sharklet™ geometry must be imposing some currently unknown thermodynamic penalty on algal adhesion that is not provided by parallel channels.

It has been shown that for physical topographies of sufficient depth (e.g., ≥3 μm), the 2x2 Sharklet™ pattern geometry is superior to equally sized channels at inhibiting the attachment density of *U. linza*.[9] Sharklet is thought to inhibit attachment to a greater degree than channels because the diagonal diamond pattern increases the pattern's tortuosity and helps to pin advancing water contact lines thus stabilizing the Cassie-Baxter wetting state. However, these diagonal cuts also allow for an increased number of attachment points, and the SEA model accurately models the spore attachment sites, experimentally confirmed, with preference along the diagonal pattern.

The chemical patterns discussed here do not possess analogous depth effects or surface wettability. The ~130 nm tall chemical patterns can be considered to be 2 dimensional with respect to the 5 μm zoospores, and they do not provide sufficient surface area increases to significantly promote attachment in a fashion similar to ≥ 5 μm deep 5x5 and 10x10 physical patterns. Furthermore, we have shown that the chemical nanotopographies do not follow the Cassie-Baxter theory and this is supported by the significantly different static water contact angles of chemical Sharklet (~100°) and physical Sharklet (~135°).

CONCLUSIONS

A RAFT photografting technique was successfully employed to graft an array of anisotropic chemical nanotopographies composed of poly(acrylamide) onto the surface of poly(dimethylsiloxane) in the geometry of parallel channels and Sharklet™. AFM analysis revealed a linear increase in the pattern height with increasing UV polymerization time and surface nanoroughness. Water contact angle data indicated that the chemical nanotopographies have minimal impact on the macroscopic wettability of the grafted surfaces and the hydrophobic PDMSe domains dominate. Anti-biofouling tests using algal zoospores of *U. linza* showed that the non-patterned poly(acrylamide) surfaces significantly inhibit fouling attachment compared to the non-grafted controls. However, patterned poly(acrylamide) surfaces had minimal impact, and the overall anti-biofouling potential of the anisotropic chemical nanotopographies remains limited. Future testing will focus on the more effective SK2x2 patterns to determine the effect of feature height and investigate potentially more effective acrylate/methacrylate chemistries (e.g., acrylic acid, hydroxyethyl methacrylate, or quaternary ammonium salts).

AUTHOR INFORMATION

Corresponding Author

*(C.K.) E-mail ckuliasha@ufl.edu; Tel +1 (865) 604 6068; ORCID 0000-0002-5260-459X

Funding Sources

The authors acknowledge the financial support for this work by the U.S. Office of Naval Research: N00014-13-1-0443 and N00014-14-1-0445 C.A.K., R.L.F., A.B.B., and N00014-13-1-0633 and N00014-16-1-2988 J.A.F., S.C.F., A.S.C.).

Notes

Anthony Brennan is the Founder and Chairman of Sharklet Technologies

ASSOCIATED CONTENT

Supporting Information. The Supporting Information is available free of charge on the ACS Publications website at DOI: XXXXXXX. Tables and figures include a table indicating FTIR peak assignments for grafted substrates, 3D AFM line scans of P(AAm)-g-PDMSe, optical images of P(AAm)-g-PDMSe, and representative line scan plots for different lateral space groups of P(AAm)-g-PDMSe substrates.

REFERENCES

(1) Townsin, R. L. The Ship Hull Fouling Penalty. *Biofouling* **2003**, *19* (SUPPL.), 9–15. https://doi.org/10.1080/0892701021000060833.

(2) Schultz, M. P. Effects of Coating Roughness and Biofouling on Ship Resistance and Powering. *Biofouling* **2007**, *23*, 331–341.

(3) Mineur, F.; Johnson, M. P.; Maggs, C. A.; Stegenga, H. Hull Fouling on Commercial Ships as a Vector of Macroalgal Introduction. *Mar. Biol.* **2006**, *151*, 1299–1307.

(4) Connelly, N. A.; O'Neill, C. R.; Knuth, B. A.; Brown, T. L. Economic Impacts of Zebra Mussels on Drinking Water Treatment and Electric Power Generation Facilities. *Environ. Manage.* **2007**, *40* (1), 105–112. https://doi.org/10.1007/s00267-006-0296-5.

(5) Callow, M. E.; Fletcher, R. L. The Influence of Low Surface Energy Materials on Bioadhesion: A Review. *Int. Biodeterior. Biodegrad.* **1995**, *34*, 333–348.

(6) Pereni, C. I.; Zhao, Q.; Liu, Y.; Abel, E. Surface Free Energy Effect on Bacterial Retention. *Colloids Surfaces B Biointerfaces* **2006**, *48* (2), 143–147. https://doi.org/10.1016/j.colsurfb.2006.02.004.

(7) Zhao, Q.; Liu, Y.; Wang, C.; Wang, S.; Müller-Steinhagen, H. Effect of Surface Free Energy on the Adhesion of Biofouling and Crystalline Fouling. *Chem. Eng. Sci.* **2005**, *60* (17), 4858–4865. https://doi.org/10.1016/j.ces.2005.04.006.

(8) Banerjee, I.; Pangule, R. C.; Kane, R. S. Antifouling Coatings: Recent Developments in the Design of Surfaces That Prevent Fouling by Proteins, Bacteria, and Marine Organisms. *Adv. Mater.* **2011**, *23* (6), 690–718. https://doi.org/10.1002/adma.201001215.

(9) Schumacher, J. F.; Carman, M. L.; Estes, T. G.; Feinberg, A. W.; Wilson, L. H.; Callow, M. E.; Callow, J. A.; Finlay, J. A.; Brennan, A. B. Engineered Antifouling Microtopographies – Effect of Feature Size, Geometry, and Roughness on Settlement of Zoospores of the Green Alga Ulva. *Biofouling* **2007**, *23*, 55–62.

(10) Sundaram, H. S.; Cho, Y.; Weinman, C. J.; Paik, M. Y.; Dimitriou, M. D.; Finlay, J.; E.Callow, M.; A.Callow, J.; J.Kramer, E.; Ober, C. K. Surface Active Zwitterionic Block Copolymer Synthesis For Antifouling Applications and Surface Characterization. *Polym. Prepr.* **2010**, *51*, 384–385.

(11) Petrone, L.; di Fino, A.; Aldred, N.; Sukkaew, P.; Ederth, T.; Clare, A. S.; Liedberg, B. Effects of Surface Charge and Gibbs Surface Energy on the Settlement Behaviour of Barnacle Cyprids (Balanus Amphitrite). *Biofouling* **2011**, *27* (9), 1043–1055. https://doi.org/10.1080/08927014.2011.625474.

(12) Gatley-Montross, C. M.; Finlay, J. A.; Aldred, N.; Cassady, H.; Destino, J. F.; Orihuela, B.; Hickner, M. A.; Clare, A. S.; Rittschof, D.; Holm, E. R.; et al. Multivariate Analysis of Attachment of Biofouling Organisms in Response to Material Surface Characteristics. *Biointerphases* **2017**, *12* (5), 051003. https://doi.org/10.1116/1.5008988.

(13) Majumdar, P.; Crowley, E.; Htet, M.; Stafslien, S. J.; Daniels, J.; VanderWal, L.; Chisholm, B. J. Combinatorial Materials Research Applied to the Development of New Surface Coatings XV: An Investigation of Polysiloxane Anti-Fouling/Fouling-Release Coatings Containing Tethered Quaternary Ammonium Salt Groups. *ACS Comb. Sci.* **2011**, *13*, 298–

309.

(14) Nie, Z.; Kumacheva, E. Patterning Surfaces with Functional Polymers. *Nat. Mater.* **2008**, *7*, 277–290.

(15) Graham, M.; Cady, N. Nano and Microscale Topographies for the Prevention of Bacterial Surface Fouling. *Coatings* **2014**, *4* (1), 37–59. https://doi.org/10.3390/coatings4010037.

(16) Decker, J. T.; Kirschner, C. M.; Long, C. J.; Finlay, J. A.; Callow, M. E.; Callow, J. A.; Brennan, A. B. Engineered Antifouling Microtopographies: An Energetic Model That Predicts Cell Attachment. *Langmuir* **2013**, *29*, 13023–13030.

(17) Carman, M. L.; Estes, T. G.; Feinberg, A. W.; Schumacher, J. F.; Wilkerson, W.; Wilson, L. H.; Callow, M. E.; Callow, J. A.; Brennan, A. B. Engineered Antifouling Microtopographies – Correlating Wettability with Cell Attachment. *Biofouling* **2006**, *22*, 11–21.

(18) Magin, C. M.; Long, C. J.; Cooper, S. P.; Ista, L. K.; López, G. P.; Brennan, A. B. Engineered Antifouling Microtopographies: The Role of Reynolds Number in a Model That Predicts Attachment of Zoospores of Ulva and Cells of Cobetia Marina. *Biofouling* **2010**, *26*, 719–727.

(19) Chung, K. K.; Schumacher, J. F.; Sampson, E. M.; Burne, R. A.; Antonelli, P. J.; Brennan, A. B. Impact of Engineered Surface Microtopography on Biofilm Formation of Staphylococcus Aureus. *Biointerphases* **2007**, *2*, 89–94.

(20) Magin, C. M.; Neale, D. B.; Drinker, M. C.; Willenberg, B. J.; Reddy, S. T.; Perle, K. M. D. La; Schultz, G. S.; Brennan, A. B. Evaluation of a Bilayered, Micropatterned Hydrogel Dressing for Full-Thickness Wound Healing. *Exp. Biol. Med.* **2016**, *241*, 986–995.

(21) Schumacher, J. F.; Aldred, N.; Callow, M. E.; Finlay, J.; Callow, J. A.; Clare, A.; Brennan,

A. B. Species-Specific Engineered Antifouling Topographies: Correlations between the Settlement of Algal Zoospores and Barnacle Cyprids. *Biofouling* **2007**, *23*, 307–317.

(22) Krishnan, S.; Weinman, C. J.; Ober, C. K. Advances in Polymers for Anti-Biofouling Surfaces. *J. Mater. Chem.* **2008**, *18*, 3405–3413.

(23) Andruzzi, L.; Senaratne, W.; Hexemer, A.; Sheets, E. D.; Ilic, B.; Kramer, E. J.; Baird, B.; Ober, C. K. Oligo(Ethylene Glycol) Containing Polymer Brushes as Bioselective Surfaces. *Langmuir* **2005**, *21* (6), 2495–2504. https://doi.org/10.1021/la047574s.

(24) Finlay, J. A.; Krishnan, S.; Callow, M. E.; Callow, J. A.; Dong, R.; Asgill, N.; Wong, K.; Kramer, E. J.; Ober, C. K. Settlement of Ulva Zoospores on Patterned Fluorinated and PEGylated Monolayer Surfaces. *Langmuir* **2007**, *24*, 504–510.

(25) Rodriguez-Emmenegger, C.; Preuss, C. M.; Yameen, B.; Pop-Georgievski, O.; Bachmann, M.; Mueller, J. O.; Bruns, M.; Goldmann, A. S.; Bastmeyer, M.; Barner-Kowollik, C. Controlled Cell Adhesion on Poly(Dopamine) Interfaces Photopatterned with Non-Fouling Brushes. *Adv. Mater.* **2013**, *25*, 6123–6127.

(26) Moustafa, M. E.; Gadepalli, V. S.; Elmak, A. A.; Lee, W.; Rao, R. R.; Yadavalli, V. K. Large Area Micropatterning of Cells on Polydimethylsiloxane Surfaces. *J. Biol. Eng.* **2014**, *8*.

(27) Callow, M. E.; Callow, J. A.; Pickett-Heaps, J. D.; Wetherbee, R. Primary Adhesion of Enteromorpha (Chlorophyta, Ulvales) Propagules: Quantitative Settlement Studies and Video Microscopy. *J. Phycol.* **1997**, *33*, 938–947.

(28) Xia, Y.; Whitesides, G. M. Soft Lithography. *Annu. Rev. Mater. Sci.* **1998**, *28*, 153–184.

(29) Ratner, B.; Hoffman, A.; Schoen, F.; Lemons, J. *Biomaterials Science: An Introduction to Materials in Medicine*, 3rd ed.; Academic Press: Oxford, UK, 2013.

(30) Kuliasha, C. A.; Fedderwitz, R. L.; Calvo, P. R.; Sumerlin, B. S.; Brennan, A. B. Engineering the Surface Properties of Poly(Dimethylsiloxane) Utilizing Aqueous RAFT Photografting of Acrylate/Methacrylate Monomers. *Macromolecules* **2018**, *51* (2). https://doi.org/10.1021/acs.macromol.7b02575.

(31) Grozea, C. M.; Walker, G. C. Approaches in Designing Non-Toxic Polymer Surfaces to Deter Marine Biofouling. *Soft Matter* **2009**, *5*, 4088–4100.

(32) Lai, J. T.; Filla, D.; Shea, R. Functional Polymers from Novel Carboxyl-Terminated Trithiocarbonates as Highly Efficient RAFT Agents. *Macromolecules* **2002**, *35*, 6754–6756.

(33) Moad, G.; Rizzardo, E.; Thang, S. H. Living Radical Polymerization by the RAFT Process-A First Update. *Australlian J. Chem.* **2006**, *59*, 669–692.

(34) Morita, M.; Koga, T.; Otsuka, H.; Takahara, A. Macroscopic-Wetting Anisotropy on the Line-Patterned Surface of Fluoroalkylsilane Monolayers. *Langmuir* **2005**, *21*, 911–918.

(35) Jansen, H. P.; Bliznyuk, O.; Kooij, E. S.; Poelsema, B.; Zandvliet, H. J. W. Simulating Anisotropic Droplet Shapes on Chemically Striped Patterned Surfaces. *Langmuir* **2012**, *28*, 499–505.

(36) Chen, Y.; He, B.; Lee, J.; Patankar, N. A. Anisotropy in the Wetting of Rough Surfaces. *J. Colloid Interface Sci.* **2005**, *281*, 458–464.

(37) Cassie, A. B. D.; Baxter, S. Wettability of Porous Surfaces. *Trans. Faraday Soc.* **1944**, *40*, 546–551.

(38) Gao, L.; McCarthy, T. How Wenzel and Cassie Were Wrong. *Langmuir* **2007**, *23*, 3762–3765.

(39) Statz, A.; Finlay, J.; Dalsin, J.; Callow, M.; Callow, J. A.; Messersmith, P. B. Algal

Antifouling and Fouling-Release Properties of Metal Surfaces Coated with a Polymer Inspired by Marine Mussels. *Biofouling* **2007**, *22*, 391–399.

(40) Kuliasha, C. A.; Finlay, J. A.; Franco, S. C.; Clare, A. S.; Stafslien, S. J.; Brennan, A. B. Marine Anti-Biofouling Efficacy of Amphiphilic Poly(Coacrylate) Grafted PDMSe: Effect of Graft Molecular Weight. *Biofouling* **2017**, *33* (3). https://doi.org/10.1080/08927014.2017.1288807.

(41) Callow, M. E.; Callow, J. A.; Ista, L. K.; Coleman, S. E.; Nolasco, A. C.; Lopez, G. P. Use of Self Assembled Monolayers of Different Wettabilities to Study Surface Selection and Primary Adhesion Processes of Green Algae (Enteromorpha). *Appl. Enviornmental Microbiol.* **2000**, *66* (8), 3249.